15TH IEA HEAT PUMP CONFERENCE
MAY 26–29, 2026 | HOFBURG
VIENNA 2026
DECARBONISATION THROUGH INNOVATION

High-Temperature Heat Pump Storage System – Demonstrator Development

Haochen Wang[a], Dimitri Nefodov[a], Felix Oestreich[a], Thorsten Urbaneck[a,*]

[a]Professorship Applied Thermodynamics, Department of Mechanical Engineering, Chemnitz University of Technology, 09111 Chemnitz, Germany

Abstract

A substantial share of non-renewable primary energy is currently consumed for industrial process heat. To reduce this energy demand, the authors developed a novel method within the KETEC project (Research Platform for Refrigeration and Energy Technology, Subproject 10) [1] for providing process heat and steam (100 °C to approx. 300 °C). The system [2] - [4] is based on a heat pump cycle. In contrast to conventional heat pumps, a vapor/liquid storage and a high-temperature storage are integrated into the system. Water was chosen as the preferred working medium because it possesses favorable thermophysical properties. The integration of vapor/liquid storage and high-temperature storage enables cyclic operation. As a result, the system is suitable for discontinuous processes. Therefore, fluctuating power levels on the heat source side (e.g., waste heat from industrial processes) as well as on the drive side (e.g., direct use of electricity from renewable energy sources) can be compensated.
This work also presents modifications of the basic process configuration. Compression and expansion stages are varied, and the use of alternative working medium is proposed and examined. The modeling and simulation are carried out using the software EBSILON®Professional [5]. This enables the calculation of coefficient of performance for heating ε_{H} for various evaporation temperatures T_0 and condensation temperatures T_{c}. A comparative evaluation of the variants is then performed. From this, important insights can be derived that contribute to the development of a demonstrator. With the planned demonstrator, the primary goal is to provide proof of function for the novel process. This work also presents the first results from transient simulations of the demonstrator (high-temperature storage). These results show that the new approach is promising as well. The high temperature storage can be charged with superheated steam, and it is also capable of supplying superheated steam.

Keywords: Heat Pump, Storage, Process Heat, Simulation, Demonstrator

1. Introduction

For the provision of process heat, water steam is used in industry as a heat transfer medium for a wide range of applications (e.g., in the food industry and chemical industry). High-temperature heat pumps are a promising technology for steam generation. To further minimize the use of fossil energy, the authors are working within the KETEC project (Research Platform for Refrigeration and Energy Technology, Subproject 10) [1] on the development of a new high-temperature heat pump storage system [2] - [4]. This contribution presents an investigation based on the work of *Urbaneck* et al. described in [4], and the next section shows additional modifications of the proposed system with a simple process configuration [2] - [4].

* Corresponding author. Tel.: +49 371 531-32463
E-mail address: thorsten.urbaneck@mb.tu-chemnitz.de

15th IEA Heat Pump Conference 2026 - HTH11.2 - https://doi.org/10.23697/4yk4-dn07

2. Configurations

Urbaneck et al. describe in [4] in detail a new heat pump storage system for the supply of process heat and steam. The simple configuration (Figure 1) is referred to here as Variant 1. Variant 1 can also be modified (Figure 2 to Figure 5).

The process (Figure 1) is comparable to a closed heat pump cycle (mechanical vapor recompression). However, an open system can also be realized. The vapor/liquid storage corresponds to the evaporator, while the high-temperature storage acts like the condenser. In practical operation, the states within the two storages are time-dependent due to heat transfer. For example, the superheated steam leaving the compressor undergoes complete or partial condensation and cooling during the charging of the high-temperature storage. During the charging of the high-temperature storage, insufficient heat input leads to a decrease in temperature and pressure in the vapor/liquid storage. These changes in turn affect the temperature and pressure at the compressor outlet.

Figure 2 shows Variant 2 with two-stage compression and expansion using a single working fluid. The number of stages can also be further increased. Multi-stage compression is suitable, for example, for higher condensation temperatures during the charging of the high-temperature storage, or for larger temperature lifts $(T_{\mathrm{c}} - T_0)$.

Through multi-stage expansion (Variant 3, Figure 3), states with low specific enthalpy can be achieved (a shift of the states toward the lower left in the lg p,h-diagram). This multi-stage expansion can also be implemented with multiple high-temperature storages and different or controlled expansion devices. To ensure comparability in the following investigation, two expansion stages were defined for the steady-state simulation.

Variant 4 (Figure 4) includes two-stage compression and two-stage expansion with an external heat exchanger (located inside or outside a vapor/liquid storage). The heat exchanger enables the use of two different working fluids. By selecting appropriate working fluids, the processes can be adapted and optimized (e.g., operation under overpressure conditions or maximization of the coefficient of performance for heating ε_{H}).

Figure 5 shows Variant 5 with an internal heat exchanger. This variant enables the preheating or superheating of the suction steam. It is intended to improve the operation condition, as the suction steam should be superheated to prevent damage to the compressor (e.g., turbo compressor liquid slugging).

To illustrate the differences among all variants more clearly, the characteristics of the variants have been summarized in Table 1.

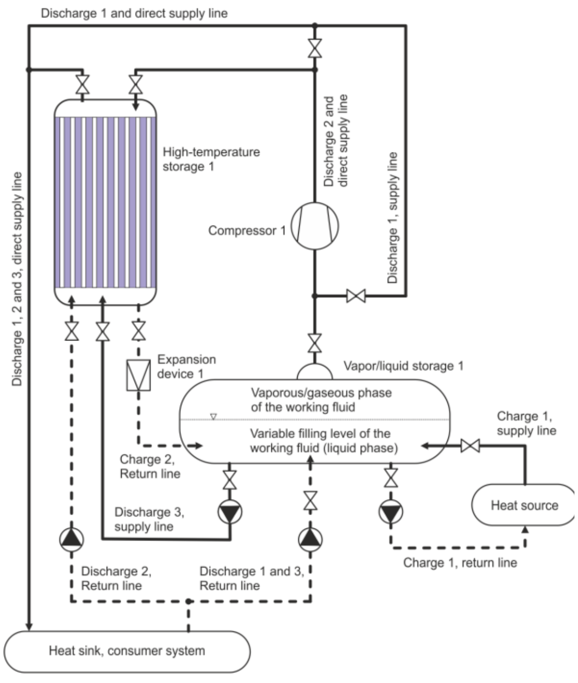

Figure 1. Variant 1, Heat pump storage system with single-stage compression, using one working fluid, one high-temperature storage, single-stage expansion, one vapor/liquid storage, and one heat source system [2] - [4]

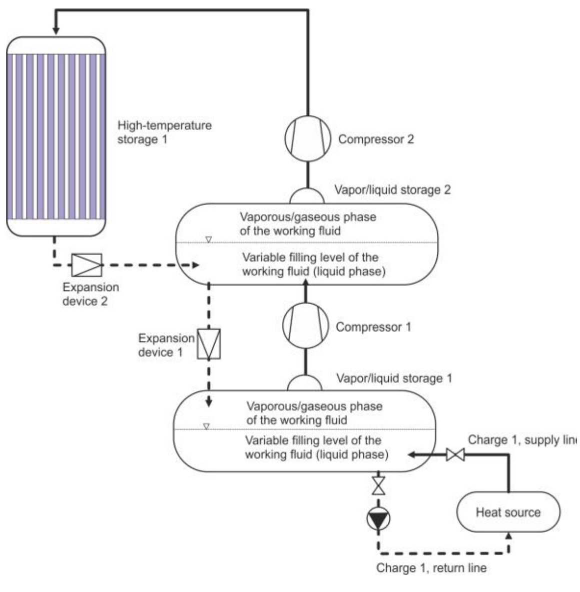

Figure 2. Variant 2, Heat pump storage system with two-stage compression, using one working fluid, one high-temperature storage, two-stage expansion, two vapor/liquid storages, and one heat source system [2] - [4]

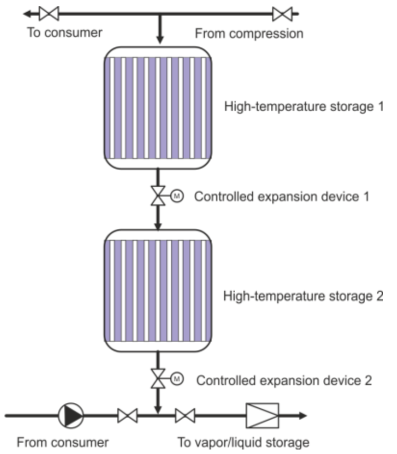

Figure 3. Variant 3, Heat pump storage system (section) with two high-temperature storages, using one working fluid, two-stage expansion[1] [2] - [4]

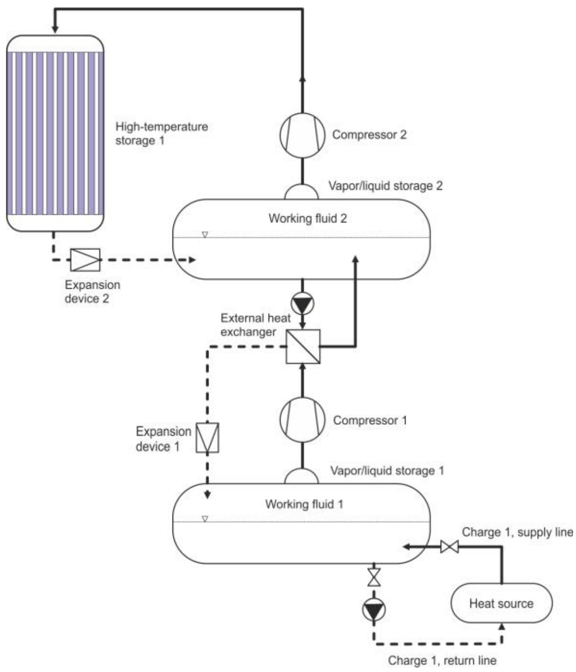

Figure 4. Variant 4, Heat pump storage system with two-stage compression, using two working fluids, one high-temperature storage, one heat exchanger, two-stage expansion, two vapor/liquid storages, and one heat-source system [2] - [4]

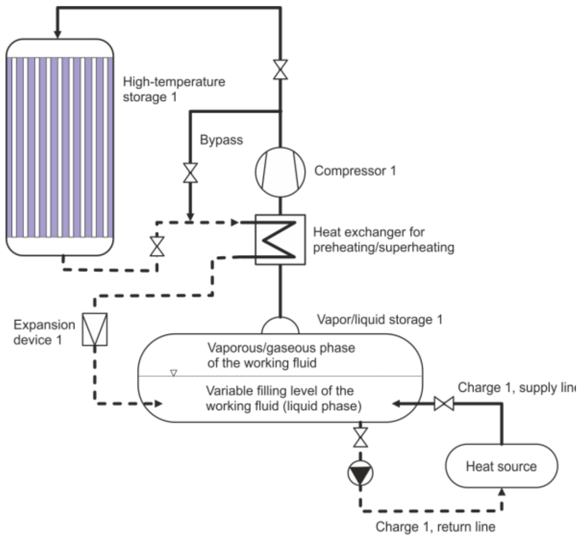

Figure 5. Variant 5, Heat pump storage system with single-stage compression, using one working fluid, one high-temperature storage, single-stage compression, one vapor/liquid storage, one heat-source system, and one heat exchanger for preheating the suction steam [2] - [4]

Table 1. Features of the five variants

	Compression	Expansion	Working fluid	Heat exchanger	Superheating
Variant 1	single-stage	single-stage	R718	-	-
Variant 2	two-stage	two-stage	R718	-	-
Variant 3	single-stage	two-stage	R718	-	-
Variant 4	two-stage	two-stage	R718/Ethanol	x	-
Variant 5	single-stage	single-stage	R718	-	x

[1] A single-stage compression is not shown in this section.

3. Steady-State Simulation of the System

3.1. Models

All transient processes were first treated in simplified form as steady-state processes. This assumption allows the following simplification: the high-temperature storage is modelled as a condenser, and the vapor/liquid storage as an evaporator. The authors assume that the working fluid (water) evaporates completely in the evaporator and fully condenses in the condenser. All components (e.g., piping, pumps) of the heat source system and the heat sink system (process heat, steam) are not taken into account in these simulations.

The energy efficiency of Variants 1 to 5 is evaluated using the coefficient of performance for heating ε_{H} Eq. (1) [10]. Table 2 summarizes the main boundary conditions for the steady-state simulations. The evaporation temperature T_0 and the condensation temperature T_{c} correspond to the temperatures on the heat source side and the heat sink side, respectively. To cover a wide range of applications, the evaporation temperature T_0 is varied from 40 °C to 120 °C in steps of 20 K. The condensation temperature T_{c} is set in the range from 140 °C to 200 °C, also in 20 K increments. The minimum temperature lift $\Delta T_{\mathrm{lift,min}}$ is defined as 20 K. With the exception of Variant 5, none of the steady-state simulations account for superheating ΔT_{SH}. The subcooling ΔT_{SC} is set to 0 K for all variants. The isentropic efficiency of the compressor $\eta_{\mathrm{Com,is}}$ and the motor efficiency η_{Mot} are set to 0.70 and 0.85, respectively [7] - [9].

Table 2. Main boundary conditions of the steady-state simulation with EBSILON®Professional [5]

T_0 [°C]	40…120
T_{c} [°C]	140…200
$\Delta T_{\mathrm{lift,min}}$ [K]	20
ΔT_{SH} [K]	0
ΔT_{SC} [K]	0
$\eta_{\mathrm{Com,is}}$ [-]	0.70
η_{Mot} [-]	0.85

$$\varepsilon_{\mathrm{H}} = \frac{\dot{Q}_{\mathrm{c,tot}}}{P_{\mathrm{Com,tot}}} \tag{1}$$

In addition to the main boundary conditions shown in Table 2, there are also specific conditions for Variants 2 to 4. For Variant 2, the intermediate pressure p_{IM} (outlet pressure of the first compression stage $p_{2,1}$) lies at the midpoint of the logarithmic pressure scale between the evaporation pressure p_0 and the condensation pressure p_{c}. This ensures that both compressors have the same compression ratio $\varepsilon_{\mathrm{Comp}}$. Variant 3 uses the same method to determine the intermediate pressure p_{IM} for the two-stage expansion. In Variant 4, an additional heat exchanger is used compared to Variant 2 to separate the two refrigerants (Cycle 1: ethanol; Cycle 2: water). In Variant 4, a minimum temperature difference of 5 K has been considered for heat transfer in the heat exchanger. The outlet temperature of the first compression stage $T_{2,\mathrm{LPS}}$ is treated as a variable in the simulation for Variant 4. This temperature was varied from 60 °C to 180 °C in steps of 20 K. In the following discussion (Section 3.2) regarding Variant 4, the authors use only the highest[2] coefficient of performance for heating ε_{H} for comparison. The simplified approach also allows the compression ratio $\varepsilon_{\mathrm{Comp}}$ and the maximum compressor outlet temperature $T_{\mathrm{Com,out,max}}$ to take values that may not be practically achievable.

3.2. Results and Discussion

The energy efficiency of the process (Variants 1 to 5) is evaluated using the coefficient of performance for heating ε_{H} Eq. (1). Figure 6 to Figure 9 show the dependence of the coefficient of performance for heating ε_{H} on the evaporation temperature T_0 and the condensation temperature T_{c}. Variants 2 and 3 yield the highest coefficient of performance for heating ε_{H}. The results of Variant 2 and Variant 3 show a similar growth behavior. The difference between the two results is negligible (less than 1% at all condensation temperatures T_{c}). Likewise, the results of Variant 1 and Variant 5 show a similar rate of increase. Again, the

[2] The coefficient of performance for heating ε_{H} refers to a fixed evaporation temperature T_0 and condensation temperature T_{c} (variable: outlet temperature of the first compression stage $T_{2,\mathrm{LPS}}$).

difference between the results is negligibly small (below 1% at all condensation temperatures T_c). Variant 4 has an advantage compared to the other four variants only when the evaporation temperatures T_0 lie in a relatively low range (40 °C to 80 °C).

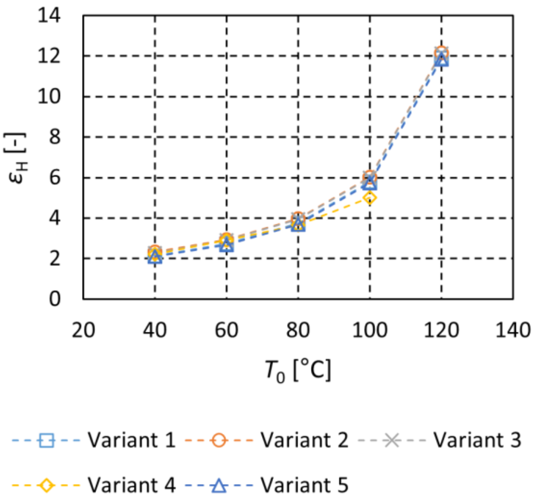

Figure 6. Dependence of the coefficient of performance for heating ε_H on the evaporation temperature T_0 at a condensation temperature T_c of 140 °C

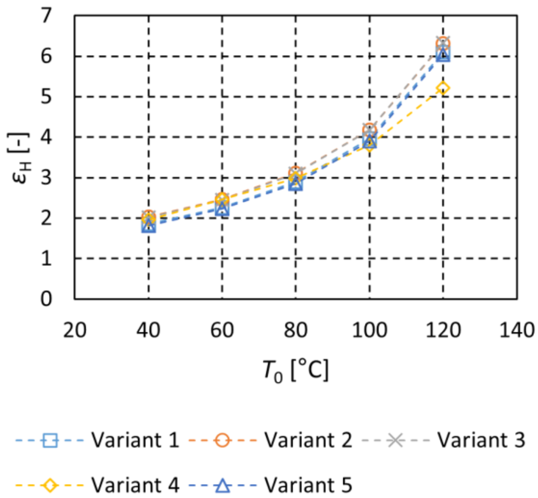

Figure 7. Dependence of the coefficient of performance for heating ε_H on the evaporation temperature T_0 at a condensation temperature T_c of 160 °C

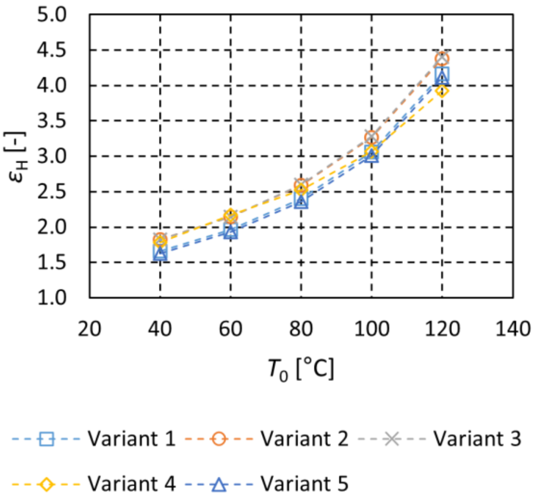

Figure 8. Dependence of the coefficient of performance for heating ε_H on the evaporation temperature T_0 at a condensation temperature T_c of 180 °C

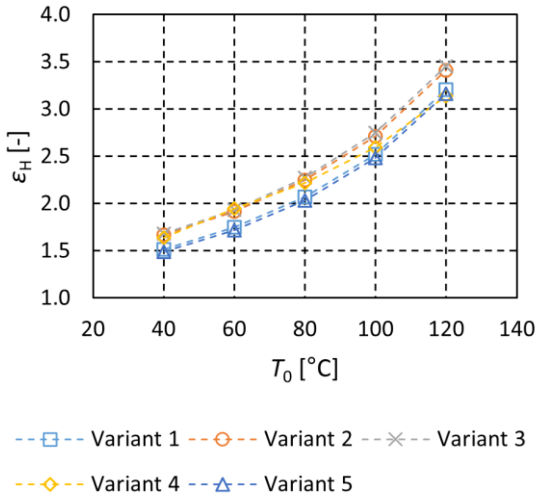

Figure 9. Dependence of the coefficient of performance for heating ε_H on the evaporation temperature T_0 at a condensation temperature T_c of 200 °C

A two-stage compression (Variant 2) practically does not result in an increase in the coefficient of performance for heating ε_H compared to single-stage compression (Variant 3) within the examined range. The isentrope in this range show an approximately linear and parallel course. This, in turn, affects the calculation of the specific compression work. As a result, the differences in the coefficient of performance for heating ε_H between single- and two-stage compression are very small.

By contrast, a two-stage expansion (Variants 2 and 3) can achieve a moderate increase in the coefficient of performance for heating ε_H compared to single-stage expansion (Variant 1). This can be explained by the flatter course of the boiling line in comparison with the dew line.

The use of two working fluids (ethanol and water) in Variant 4 requires a heat exchanger for fluid separation. The assumed minimum temperature difference of 5 K in the heat exchanger has a generally negative effect on the coefficient of performance for heating ε_H, due to the higher condensation temperature of ethanol. Nevertheless, Variant 4 provides higher coefficient of performance for heating ε_H compared with Variant 1 at low heat-source temperatures (40 °C to 80 °C). At large temperature differences between the heat source and the heat sink, the impact of the heat exchanger becomes less significant.

Variant 5 shows no advantages in terms of the coefficient of performance for heating ε_{H} compared with the other variants. In practical operation, however, this variant ensures superheating at the compressor inlet, which can prevent liquid slugging in the compressor.

The results generally show that high coefficient of performance for heating ε_{H} can be achieved with the proposed process. The maximum coefficient of performance for heating ε_{H} is 1.68 at a large temperature lift (ΔT_{lift} = 160 K; Variant 3: T_0 = 40 °C, T_{c} = 200 °C) and 12.15 at a small temperature lift (ΔT_{lift} = 20 K; Variant 2: T_0 = 120 °C, T_{c} = 140 °C). A high coefficient of performance for heating ε_{H} allows for greater flexibility in responding to changes in electricity procurement costs for constant heat generation costs [6]. This supports flexible operation for the system operator as well.

However, when applying these variants in practice, technical limitations arise, such as the compression ratio $\varepsilon_{\mathrm{Comp}}$ and the maximum compressor outlet temperature $T_{\mathrm{Com,out,max}}$. In the field of steam compression, the compression ratio $\varepsilon_{\mathrm{Comp}}$ is typically below 2.5, and the maximum compressor outlet temperature $T_{\mathrm{Com,out,max}}$ is generally limited to approximately 250 °C [7] - [9].

4. Transient Simulation of the High-Temperature Storage

To better understand and evaluate the functionality of the high-temperature heat pump storage system, the high-temperature storage is modelled separately because it plays a significant role in the whole system. EBSILON®Professional [5] was used to analyse the charging and discharging processes of the high-temperature storage. This section refers to the under-construction demonstrator (TP10-Demonstrator). The demonstrator is presented in Section 5. Thus, this section also provides preliminary investigations for the TP10-Demonstrator.

4.1. Structure and Function

A schematic representation of the high-temperature storage is shown in Figure 10. Iron rods are used as storage elements or storage material inside the high-temperature storage. During the charging process, the superheated steam exiting the compressor enters the high-temperature storage from the top. The superheated steam encounters the storage elements (iron rods) with a lower temperature. Through heat transfer (storage charging), the steam cools down and condenses.

During the discharging process, liquid water (condensate) from the vapor/liquid storage, at a temperature slightly below the boiling temperature, is fed into the bottom of the high-temperature storage. Upon contact with the heated iron rods, the water is first heated to its boiling temperature and then evaporates. Ideally, the steam becomes superheated and flows out of the high-temperature storage at the top.

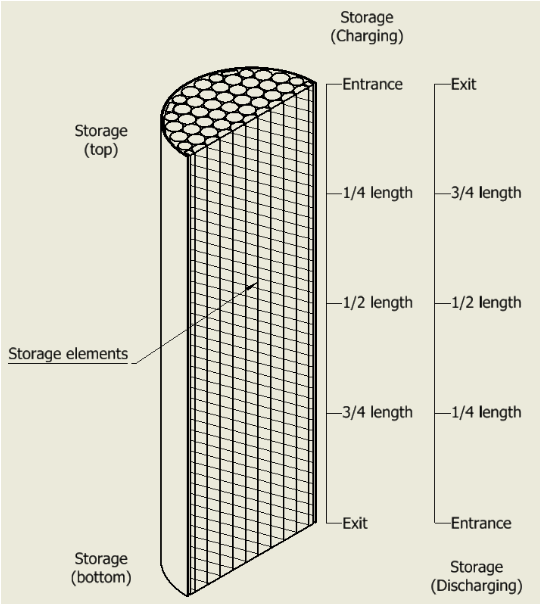

Figure 10. Schematic representation of a section of the high-temperature storage, including the charging and discharging directions as well as the relative lengths of the storage elements (section view without storage cover, connections, thermal insulation, casing, measurement equipment, etc.)

4.2. Simulation Settings and Assumptions

For modelling the high-temperature storage, the EBSILON component 165 (Thermal regenerator/Bulk material storage) is used [5]. Table 3 lists the main configurations of the transient simulation (high-temperature storage). The inlet temperature during charging $T_{\mathrm{HTS,CH,in}}$ and the inlet temperature during discharging $T_{\mathrm{HTS,DCH,in}}$ correspond to the compressor outlet temperature (190 °C) and the return temperature on the heat sink side (115 °C), respectively. The inlet pressure during charging $p_{\mathrm{HTS,CH,in}}$ and during discharging $p_{\mathrm{HTS,DCH,in}}$ are 2.70 bar and 1.69 bar. The length of the high-temperature storage l_{HTS} and the length of the storage elements l_{SE} are both set to 1500 mm to simplify the simulation. The initial temperature of the storage elements $T_{\mathrm{HTS,CH,start}}$ is defined as 115 °C.

When designing the high-temperature storage, the authors attempted to keep the porosity as low as possible in order to increase the storage capacity. Therefore, the high-temperature storage of the TP10-Demonstrator uses 85 iron rods with a diameter d_{SE} of 50 mm as storage material. The high-temperature storage has an inner diameter d_{HTS} of 500 mm. Without considering additional constructive features, this results in a porosity ε_{P} of 0.17 and a surface-to-volume ratio $A_{\mathrm{SE}}/V_{\mathrm{SE}}$ of 81 1/m. Another important assumption in the simulation is that the mass flow rate at the inlet and outlet of the high-temperature storage are equal. A charging cycle $t_{\mathrm{HTS,CH}}$ of 2.0 hours is modelled. The subsequent discharging phase $t_{\mathrm{HTS,DCH}}$ lasts 0.5 hours.

Table 3. Main configurations of the transient simulation (high-temperature storage) using EBSILON®Professional [5]

$T_{\text{HTS,CH,in}}$ [° C]	190
$p_{\text{HTS,CH,in}}$ [bar]	2.70
$T_{\text{HTS,DCH,in}}$ [° C]	115
$p_{\text{HTS,DCH,in}}$ [bar]	1.69
l_{HTS} [mm]	1500
d_{HTS} [mm]	500
l_{SE} [mm]	1500
d_{SE} [mm]	50
$\varepsilon_{\text{P,HTS}}$ [-]	0.17
$A_{\text{SE}}/V_{\text{SE}}$ [1/m]	81
$T_{\text{HTS,CH,start}}$ [° C]	115
$t_{\text{HTS,CH}}$ [h]	2.0
$t_{\text{HTS,DCH}}$ [h]	0.5

4.3. Results and Discussion

Figure 11 to Figure 14 show the simulation results for the charging and discharging cycle. Figure 11 and Figure 12 present the outlet temperature $T_{\text{HTS,out}}$ and the vapor quality $x_{\text{HTS,out}}$ of the medium leaving the high-temperature storage over a period of 2.5 hours. It can be seen that condensate flows out of the bottom of the storage until approximately 0.25 h, after that wet steam flows out. This means that from this point onward, the incoming superheated steam is no longer fully condensed. After 0.75 h, almost all saturated steam exits the high-temperature storage, and the condensation process is clearly greatly reduced. The heat transfer from the superheated steam to the storage elements occurs largely without phase change. The temperature of the storage elements increases continuously from top to bottom (Figure 10 and Figure 13). However, the outlet temperature of the high-temperature storage $T_{\text{HTS,out}}$ remains at around 130 °C for approximately 1.8 h, which is close to the condensation range (condensation temperature T_c corresponding to the inlet pressure $p_{\text{HTS,CH,in}}$ of 2.70 bar). Only after this point is a slight increase observed. This supports the assumption that saturated-steam conditions persist in the lower region of the storage unit for a long time. At the end of the charging phase at $t = 2.0$ h, the temperature difference between the upper and lower ends of the storage elements is about 60 K.

During the time period from 2.0 h to 2.5 h, the high-temperature storage is discharged. Liquid water close to its boiling point ($T_{\text{HTS,DCH,in}}$) enters the lower part of the storage at 115 °C. During both charging and discharging, the authors use the same mass flow rate (Figure 10). The incoming water first encounters the cooler lower region of the storage elements at about 130 °C and evaporates there. The saturated steam then flows upward. During this process, the saturated steam continuously absorbs thermal energy from the storage element. Figure 13 shows the superheated steam can reach approximately 185 °C, which can be observed for about 0.3 h. After this period, the high-temperature storage supplies only wet steam at around 115 °C.

The simulation results also show that the high-temperature storage can store approximately 40 kWh of heat during this period. Figure 14 illustrates the energy flow in the high-temperature storage $\dot{Q}_{\text{HTS}}$ during the charging and discharging processes. The maximum transferred power is about 108 kW for both charging and discharging. The period of maximum power shown in Figure 14 corresponds to the phase-change periods shown in Figure 11 and Figure 12. This once again highlights the characteristic operational behavior of the high-temperature storage.

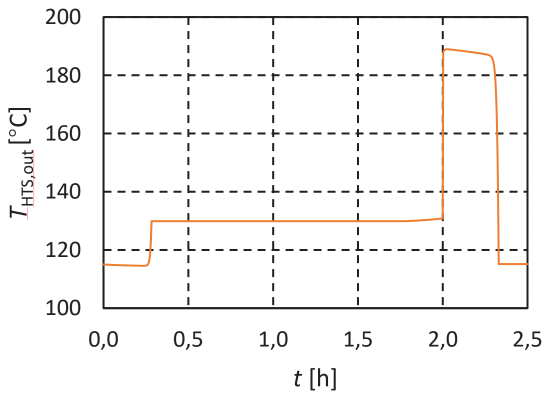

Figure 11. Outlet temperature of the high-temperature storage $T_{\text{HTS,out}}$

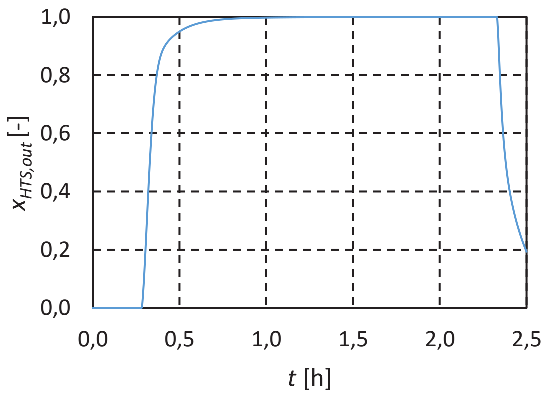

Figure 12. Vapor quality at the outlet of the high-temperature storage $x_{\text{HTS,out}}$

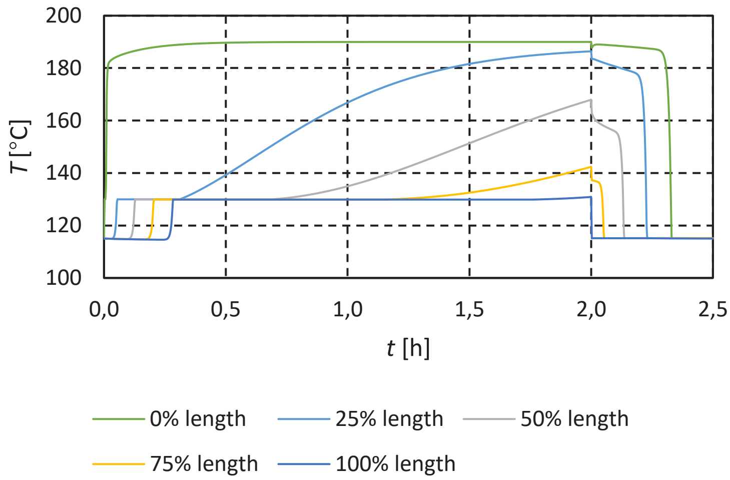

Figure 13. Temperature profile in the storage elements of the high-temperature storage at different positions

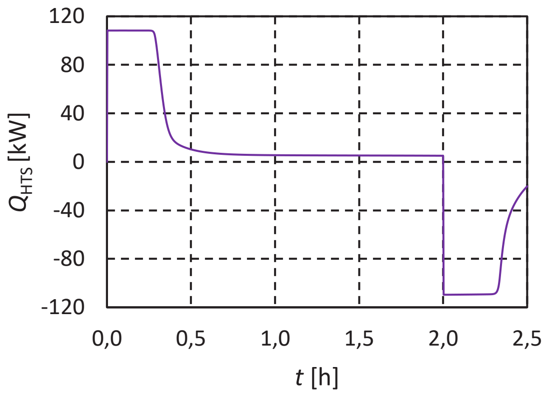

Figure 14. Energy flow in the high-temperature storage $\dot{Q}_{HTS}$

5. Construction of a Test Rig

Based on the concept presented above [2] - [4] and the obtained results, the authors are currently constructing a demonstrator (TP10-Demonstrator) within the KETEC project (Research Platform for Refrigeration and Energy Technology, Subproject 10) [1]. This demonstrator is intended to provide proof of functionality and demonstrate technical feasibility. Furthermore, an optimization of the process operation is planned. The measurement data will subsequently be used for validating the simulation models, which in turn enables improved system design.

To simplify the setup of the demonstrator and to increase operational safety, Variant 1 (Figure 1) was selected as the basis of the demonstrator. Figure 15 shows a 3D representation of the under-construction demonstrator (visualized using AutoCAD Plant 3D [11]). An electric heating rod is installed in the vapor/liquid storage to simulate the heat source system. During the discharging of the high-temperature storage, the steam will be directed back into the vapor/liquid storage. A cooling unit will be used to dissipate the heat (not shown in Figure 15).

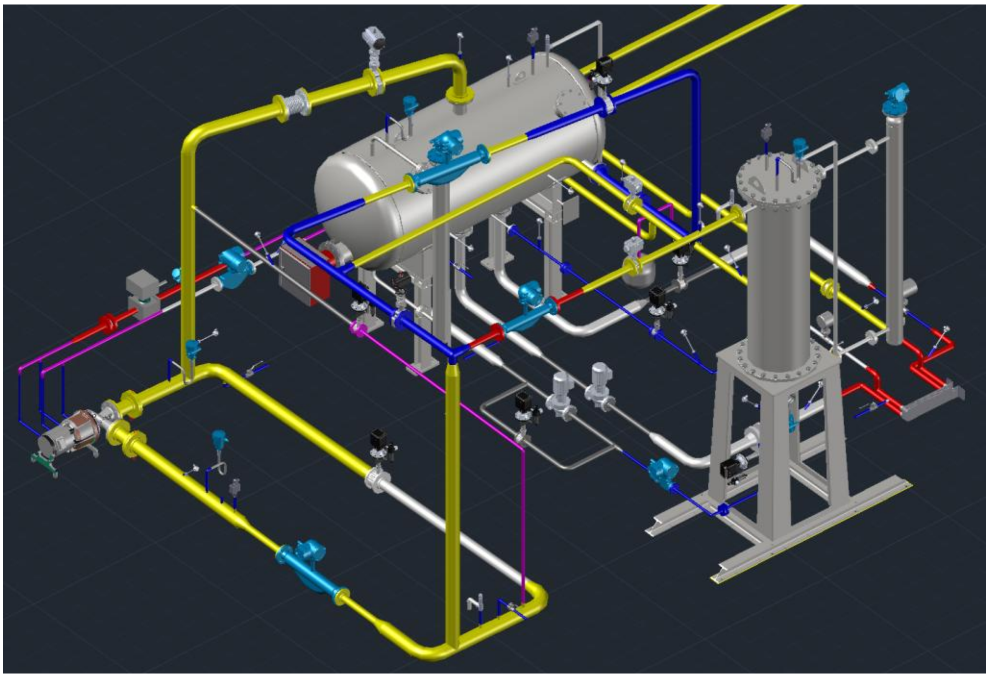

Figure 15. 3D representation of the under-construction demonstrator (TP10-Demonstrator)

6. Conclusion

Urbaneck et al. describe in detail a novel heat-pump storage system in [4]. This heat-pump storage system differs from existing solutions through the combination of a vapor/liquid storage with a high-temperature storage. The transfer of thermal energy between the two storages is carried out by means of mechanical vapor recompression. In principle, high condensation temperatures T_c, large temperature lifts ΔT_{lift}, and high coefficient of performance for heating ε_{H} (up to approx. 12) can be achieved. The simple process configuration or the basic system can be modified (e.g., multi-stage compression and expansion). However, the multi-stage process did not lead to any significant increase in the coefficient of performance for heating ε_{H}. The process also allows the use of multiple working fluids, which may be advantageous at large temperature lifts ΔT_{lift} or at low heat source temperatures T_{HSo}. Additionally, measures (e.g., suction-side superheating) can be implemented to ensure safe operation. Table 4 summarizes the advantages of the various variants.

Table 4. Summary of the advantages of the variants

	Simple construction	Improvement ε_{H}	Improvement $\varepsilon_{\mathrm{Comp}}$	Low T_0	High T_c
Variant 1	x	-	-	-	x
Variant 2	-	x	-	-	x
Variant 3	-	x	-	-	x
Variant 4	-	-	x	x	x
Variant 5	-	-	-	-	x

The transient simulation of the high-temperature storage shows that heat can be stored at a high temperature level (approx. 190 °C) and later supplied as superheated steam to a consumer system. This represents a significant advantage over conventional steam accumulators and hybrid storage systems. Due to the comparatively good results for the single-stage process (Variant 1, Figure 1) and its demonstrated advantages (e.g., simple setup), this configuration is being implemented for the first time in a demonstrator. Within the KETEC project (Research Platform for Refrigeration and Energy Technology, Subproject 10) [1], the authors are developing this process and the associated heat-pump storage systems [2] - [4] further. The authors see great application potential in the district heating sector as well as in industrial process heat supply.

Acknowledgements

The underlying collaborative project is funded by the Federal Ministry of Research, Technology and Space (BMFTR) under project numbers 03SF0623A/B/C, based on a resolution of the German Bundestag. The project is managed by Project Management Jülich (PtJ). The responsibility for the content of this publication lies with the authors. The authors expressly thank the funding agency and all partners for their support and cooperation.

Nomenclature

Symbols

A/V	Surface-to-volume ratio [1/m]
d	Diameter [mm]
h	Specific enthalpy [kJ/kg]
l	Length [mm]
p	Pressure [bar]
P	Electric power [kW]
$\dot{Q}$	Thermal capacity [kW]
T	Temperature [°C]
x	Vapor quality [-]
ε_{H}	Coefficient of performance for heating [-]
ε_{P}	Porosity
$\varepsilon_{\mathrm{Comp}}$	Compression ratio [-]
η	Efficiency ratio [-]

Indices

0	Evaporation
C	Condensation
CH	Charge
Com	Compressor
Comp	Compression
DCH	Discharge
HPS	High pressure stage
HSi	Heat sink
HSo	Heat source
HTS	High-temperature storage
IM	Intermediate
in	Inlet
is	Isentropic
lift	Lift
LPS	Low pressure stage
max	Maximum
min	Minimum
Mot	Motor
out	Outlet
SC	Subcooling
SH	Superheating
tot	Total

References

[1] Urbaneck, T.; Matthes, M.; Richter, M.; Hempel, O.; Safarik, M.; Franzke, U.; Noack, R.; Honke, M.; Müller, M.; Henninger, S.; Schossig, P.; Henning, H.-M.; de Oliveira, H. T.; Morgenstern, A.; Nienborg, B.; Gschwander, S.; Engelmann, P.; Benndorf, G.: www.ketec.online. Internetseite zum Verbundvorhaben 14.11.2025.

[2] Urbaneck, T.; Nefodov, D.; Wang, H.: Anlage und Verfahren zur Energie- und/oder Stoffversorgung mindestens eines Verbrauchers. DE 10 2023 117 382.0, Patentanmeldung vom 30.06.2022

[3] Urbaneck, T.; Nefodov, D.; Wang, H.: Anlage und Verfahren zur Energie- und/oder Stoffversorgung mindestens eines Verbrauchers. DE 20 2023 103 656, Gebrauchsmusteranmeldung vom 30.06.2022, Eintragung am 22.08.2023

[4] Urbaneck, T.; Nefodov, D., Wang, H., Oestreich, F.: Wärmepumpen-Speicher-Systeme für die Dampfversorgung – Vorstellung des Konzeptes. KI – Kälte-, Luft- und Klimatechnik, Hüthig 60. Jg. (2024) Heft 6-7 S. 48-54. – ISSN 1865-5432

[5] STEAG Energy Services GmbH, 2024. EBSILON Professional 16.04.

[6] Wang, H.; Nefodov, D.; Richter, M.; Urbaneck, T.: Bereitstellung von Prozesswärme mit Wärmepumpen und Fernwärme. EuroHeat&Power, VDE Verlag 53. Jg. (2024), Heft 3, S. 33-41. - ISSN 0949-166X

[7] Zühlsdorf, B.; Schlemminger, C.; Bantle, M.; Evenmo, K.; Elmegaard, B.: Design recommendations for R-718 heat pumps in high temperature applications, 13th IR Gustav Lorentzen Conference, Valencia, 2018. International Institute of Refrigeration. DOI https://doi.org/10.18462/iir.gl.2018.1367
[8] Bantle, M.; Schlemminger, C.; Gabrielii, C.; Ahrens, M.: Turbo-compressors for R718: Experimental evaluation of a two-stage steam compression cycle, 2019. DOI 10.18462/iir.icr.2019.0973
[9] Bantle, M.: Turbo-compressors: Prototype tests of mechanical vapour recompression for steam driers, 12th IEA Heat Pump Conference, 2017
[10] Arpagaus, C.: Hochtemperatur-Wärmepumpen Marktübersicht; Stand der Technik und Anwendungspotenziale. VDE Verlag GmbH, Berlin, Offenbach, 2019. – ISBN 978-3-8007-4550-0.
[11] Autodesk: AutoCAD Plant 3D, 2024.